fractal and fractional

MDPI

Article

Local Singularity Spectrum: An Innovative Graphical Approach for Analyzing Detrital Zircon Geochronology Data in Provenance Analysis

Wenlei Wang [1,*], Yingru Pei [1], Qiuming Cheng [2] and Wenjun Wang [3]

[1] Institute of Geomechanics, Chinese Academy of Geological Sciences, Beijing 100081, China
[2] State Key Lab of Geological Processes and Mineral Resources, China University of Geosciences (Beijing), Beijing 100083, China
[3] Henan Fourth Geological Exploration Institute Co., Ltd., Zhengzhou 450001, China
* Correspondence: wenleiw@163.com

Abstract: Detrital zircon geochronology plays a crucial role in provenance analysis, serving as one of the fundamental strategies. The age spectrum of detrital zircons collected from the sedimentary unit of interest is often compared or correlated with that of potential source terranes. However, biases in the age data can arise due to factors related to detrital sampling, analysis techniques, and nonlinear geological mechanisms. The current study reviewed two sets of detrital zircon datasets established in 2011 and 2021 to discuss the origins of the Tibetan Plateau. These datasets collected from different media effectively demonstrate a progressive understanding of provenance affinity among the main terranes on the Tibetan Plateau. This highlights issues regarding weak and unclear temporal connections identified through analyzing the age spectrum for provenance analysis. Within this context, a local singularity analysis approach is currently employed to address issues associated with unclear and weak provenance information by characterizing local variations in nonlinear behaviors and enhancing detection sensitivity towards subtle anomalies. This new graphical approach effectively quantifies temporal variations in detrital zircon age populations and enhances identification of weak provenance information that may not be readily apparent on conventional age spectra.

Keywords: U-Pb age; nonlinearity; geochronology; weak anomaly; singularity

Citation: Wang, W.; Pei, Y.; Cheng, Q.; Wang, W. Local Singularity Spectrum: An Innovative Graphical Approach for Analyzing Detrital Zircon Geochronology Data in Provenance Analysis. *Fractal Fract.* **2024**, *8*, 64. https://doi.org/10.3390/fractalfract8010064

Academic Editor: Viorel-Puiu Paun

Received: 18 December 2023
Revised: 11 January 2024
Accepted: 11 January 2024
Published: 17 January 2024

1. Introduction

Sedimentary rocks occupy 66% (±3.5%) of the exposed rocks on the Earth's surface, preserving significant geo-information descriptive of the geological evolution [1]. Detrital zircons as typical components in sedimentary rocks inheriting stable physical and chemical properties of igneous zircon are ubiquitous and observable in clastic sediments after multiple sedimentary cycles and/or tectonothermal events [2,3]. Due to the high closure temperature of the U-Th-Pb isotopic system, the age spectrum of detrital zircons can still reflect the age composition of rocks in the source areas of sediments even after weathering, migration, and deposition [4]. Provenance analysis is one of the most common applications of detrital zircon geochronology, which can reconstruct parent rock assemblages of zircon-bearing sediments and their forming environment [5]. The fundamental strategy of the conventional detrital zircon U-Pb geochronology approach in provenance analysis is to compare or correlate the age spectra of detrital zircons collected from the sedimentary unit of interest (e.g., a river, soil, and/or sedimentary rocks) with that of ancient sediments and/or crystalline (i.e., igneous and metamorphic) rocks developed in adjacent orogenic belts or other possible source terranes [6]. Similar or comparable age peaks observed in samples from different locations can provide initial indications of

potential provenance affinity among these samples. The establishment of stationary provenance connections in support of paleogeography reconstruction, tectonic evolution, and other provenance-related issues is further supported by comparable Hf isotopic data and concurrent magmatic and/or metamorphic activities [7–10]. The analysis of age spectrum correlation is crucial in examining the similarities and differences among spectra of various samples. That enables to determine whether these samples originate from or are influenced by different provenance systems.

Accompanied by fast development in in situ microanalytical dating techniques in recent decades, detrital zircon U-Pb geochronology has been broadly promoted, and U-Pb age data accumulated fast and significantly increased either in quantity or quality. Many detrital zircon U-Pb age databases were established worldwide [11]. According to more delicate sampling and spectrum correlation among samples from various media and locations, detrital zircon age spectrum-based approaches can be further utilized in quantifying sediment budgets of rivers [12], modeling terrane displacement [8], characterizing subduction erosion, underplating [13] and ultrahigh-pressure metamorphism [14], and reconstructing paleogeography [15]. Peaks and troughs on these age spectra at both local and global scopes were identified to discuss correlations between a supercontinent and a superplume that further support the proposition of the episodic evolution model of the continental crust [16,17]. The limitation in comprehensive provenance information mining has now been conspicuously improved and mitigated.

The effective management and manipulation of these "big data" pose a novel challenge in advancing provenance analysis. It has been revealed that numerous geological and sampling issues may influence the application and discussion of zircon age data. First of all, zircon-bearing igneous rocks can be influenced by plate movement and may experience different weathering and preservation processes. Precise analysis of continental evolution through intensity changes on zircon age spectra might be inappropriate due to influences of sampling heterogeneity and representativeness of samples [18]. Secondly, differences in zircon fertility and preservation among various tectonic settings, and spatial distribution of detrital zircons after sedimentary cycles and/or tectonothermal events might be heterogenetic. Detrital zircon-bearing samples are often dispersed, which may further enhance the heterogeneity to some extent. Thirdly, the number of analyses for individual samples is often lower than the quality required for statistical significance [19]. Some progressive studies found that the increase in detrital zircon age data does not always improve the solution of geological issues, and in some cases, they may become more complicated and difficult [16]. Age spectrum correlation is facing issues of weak anomaly or weak information.

New progress brings new demand on data visualization and interpretation methodology for better utilization of both reported and future geochronology datasets. At this point, possible inherent bias intrinsic to data acquisition and analysis methods of detrital zircon data should be reviewed to verify if more delicate manipulations to reveal latent rules are necessary. Within the context of weak anomalies and/or weak information discussed above, the current study applies local singularity analysis to two published detrital zircon age datasets regarding the affinity of the Lhasa and Australian terranes. Reviews of previous studies focusing on detrital zircon-based provenance analysis encompassed procedures such as sampling, laboratory analysis, data visualization, and information mining. Subsequently, discussions are centered on the singularity age spectra derived from two specific datasets in order to evaluate the advantages of the singularity theory in characterizing subtle anomalies. The present study investigates and introduces a novel graphical approach into the existing framework of detrital zircon age spectrum comparison, which is objective in enhancing the capability of traditional provenance analysis to identify and discover potential provenance relationships. These two datasets are referenced because their conclusions have undergone rigorous deliberation and wide acceptance within the geological community. By utilizing these data, the effectiveness and practicality of the new method can be more accurately validated.

2. Potential Biases in Detrital Zircon Geochronological Data Analysis

The field of detrital zircon U-Pb geochronology has made significant advancements in recent decades, particularly in relation to provenance analysis [5,20]. Extensive discussions have taken place regarding influencing factors on age data quality, aiming to improve accessibility and facilitate comprehensive analysis of provenance information [19–21]. The present study provides a comprehensive review of potential biases arising from factors related to the geological mechanisms (e.g., formation and preservation) of zircons, as well as the analysis of age data (e.g., sampling, dating, visualization, and interpretation). Based on this review, unavoidable issues for improving the manipulation of existing and future age data are discussed.

2.1. Sampling and Data Analysis

The collection of zircon-bearing sedimentary samples strictly follows scientifically sound and logical criteria to establish a strong theoretical and physical basis for subsequent data analysis. Consideration is given to various literature sources that discuss the selection criteria related to sample medium, grain size, and minimum quantity of grains. When it comes to choosing the sample medium, detrital zircon-bearing sediments are typically obtained from representative stratigraphic sections as well as exposed sedimentary rock formations [22,23]. For instance, samples obtained from stratigraphic sections within a vertical range are employed to quantitatively evaluate the correlation and variation in provenances during geological periods, thereby investigating the evolution of basins and denudation history in orogenic belts [22], while samples collected from different positions within the same sedimentary layer at a lateral scale serve to objectively discern spatial variations in provenance relationships across space, supporting the reconstruction of paleogeographic environments and/or paleocurrent directions [23]. The collection of detrital zircon samples is often characterized by sparsity and discreteness, necessitating a high level of representativeness in sampling to partially mitigate biases arising from limited sample quantity. This is particularly crucial when analyzing the provenance of a regional area and/or an entire stratigraphic period [22,23].

The subsequent concern lies in the selection of grains (e.g., grain size and quantity) to ensure the absence of biases after sample preparation. It has been reported that zircon grains crystallized in igneous and metamorphic rocks exhibit variations in terms of their size and shape [24]. During the process of deposition and transportation, hydrodynamic forces can induce differential separation of zircon grains, leading to variations in the size distribution of deposited zircons at a local scale. Consequently, neglecting grain size and quantity during grain selection would compromise the representativeness of grains and the reliability of obtained provenance information. In most cases, random grain selection is preferred to avoid bias caused by size factors (e.g., magnetic separation). However, if manual separation becomes necessary due to restrictions, the selection process should consider parameters such as size, color, shape, roundness, etc. Specifically, grains smaller than the beam diameter of dating instruments and those with fractures should be excluded since their ages are unreliable and even unmeasurable. Moreover, determining the minimum number of zircon grains to be selected from a sample containing zircons is another crucial consideration, as variations in provenance information can arise from different quantities of grains. The practice of selecting 60 grains from individual sediment samples was widely employed [25]; however, statistical experiments have shown that only 5% of the grains in such a sample can be confidently identified with a 95% chance of accuracy [26]. It has been suggested that using 100 grains per sample is sufficient to identify the main age components preserved by the sample, and using 117 grains ensures the identification of every 5% age component [19]. Furthermore, not all obtained ages and age clustering based on zircon dating can be considered reliable evidence for provenance connections. Verifying an age component requires at least four to six grain ages as supporting evidence; otherwise, it may lack persuasiveness [27]. The selection of U-Pb isotopic dating techniques also plays a crucial role in the overall analytical process. The

three primary isotopic dating techniques include thermal ionization mass spectrometry (TIMS), secondary ionization mass spectrometry (SIMS), and laser ablation with inductively coupled plasma mass spectrometry (LA–ICPMS). Considering technological superiority and cost factors, TIMS, with a higher precision and accuracy, is suitable for time scale-focused studies, such as determining the intrusion age of ancient magmatic events. SIMS, with a higher spatial resolution and minimal sample loss, is appropriate for minerals exhibiting fine growth and/or oscillatory zoning. LA–ICPMS, offering the highest testing speed and an error range of 1–2%, fulfills the requirements for analyzing large amounts of data in provenance analyses and fundamental geological surveys [8,28].

Following the process of sampling and laboratory analysis, the obtained U-Pb geochronology data can be further examined using graphical approaches to characterize age distributions for interpreting provenance information. By analyzing peaks and troughs on the age spectrum (Figure 1), it becomes possible to identify the main preserved age components, which can then be utilized for correlating ages with crystalline or sedimentary rocks in potential provenance areas. In detrital zircon age-based provenance analysis, fundamental graphical approaches for age spectra include histograms, probability density plots (PDPs), kernel density estimates (KDEs), and cumulative age distribution (CAD). The plotting of histograms, which represent the distribution of measured zircon ages (y) within different age intervals (x), is a straightforward and effective graphical method. However, it is important to note that the appearance of the age spectrum in histograms can be influenced by the chosen bin widths. In other words, the depiction of the age spectrum through histograms relies on scales of measurement, specifically the bin width. Additionally, alternative representations such as probability density plots (PDPs) or kernel density estimates (KDEs) can further illustrate the age frequency distribution curves. The mathematical similarity between the basic models of PDPs and KDEs has been established [29]. The probability density $f(t)$ can be achieved through kernel smoothing or kernel density estimation, assuming that each analysis of zircon grains adheres to a Gaussian kernel.

$$f_E(t) = \frac{1}{n}\sum_{i=1}^{n} \frac{1}{\sigma_i\sqrt{2\pi}} e^{\frac{-(t-t_i)^2}{2\sigma_i^2}} \quad (1)$$

where $f_E(t)$ is an empirical estimate of the probability density function $f(t)$ for the age spectrum. t_i denotes the observed age of the ith zircon grain and n represents the population of analyzed zircons. The parameter σ_i is a predefined bandwidth assigned to all zircon grains, which governs the smoothness of the age spectrum. In a PDP, σ_i corresponds to observed analytical errors of each zircon grain, enabling simultaneous demonstration of both age distribution and analytical uncertainty. The practical application of a PDP to large sample data may lead to an increased interpretation bias due to the overlapping effect of age components [21,30]. The definition of σ_i in KDEs can be a constant or can correspond to other smoothing factors applied to zircons within a local or global range of age. However, the bandwidth contributes to a smoothing effect on the spectrum, potentially eliminating small peaks and irregularities that could provide valuable clues about provenance information [29]. A proposal suggests that both PDPs and KDEs should only be used in simple and qualitative visualization [29]. For more complex scenarios, additional mathematical treatments are required [21,30]. As an alternative to PDPs and KDEs, the cumulative age distribution (CAD) represents the cumulative distribution function of zircon ages for $t \geq 0$ in the probability domain [0, 1]:

$$F(t) = \int_0^t f(t)\mathrm{d}t \quad (2)$$

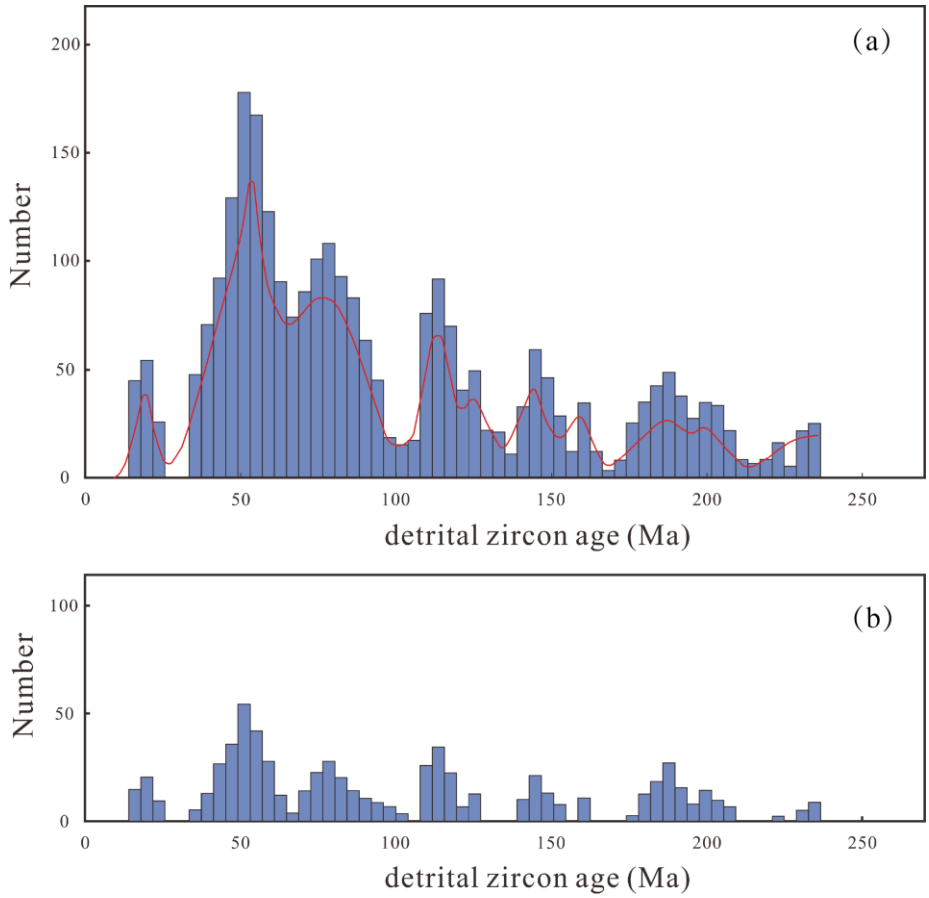

Figure 1. Schematic diagrams of detrital zircon age spectrum data delineated by probability density plots demonstrating peaks and troughs (**a**) and anomalies (**b**) separated from background by the red curve.

With increasing age, the cumulative probability curve effectively represents the likelihood of zircon being younger than a specific age. Generally, both a PDP and a CAD provide similar information; however, a PDP is more intuitive for detecting the presence or absence of a particular age component, while a CAD excels in illustrating similarities or differences among a series of age distributions. Nevertheless, interpreting subtle distinctions solely based on a simplified spectrum correlation can be challenging. This challenge becomes even more pronounced when conducting provenance analyses over large spatial scales and/or high-resolution sequence stratigraphic correlations due to the abundance of samples involved. Therefore, it is necessary to employ advanced quantitative indices to objectively describe similarities and/or differences among age distributions in various samples for quantitative correlation purposes. Examples include quantitative similarity and/or difference analyses based on nonparametric hypothesis testing, multi-dimensional scaling (MDS), and principal component analysis [21,29,30].

2.2. Geological Mechanism

The geological mechanism of detrital zircons is a significant factor influencing the identification of provenance information, in addition to the proper treatment of sampling, laboratory dating, and quantitative analytical methods. It should be noted that only well-preserved crystallization of zircon grains triggered by appropriate thermal events can be sampled and analyzed. Due to variations in zircon fertility and preservation conditions among igneous rocks, the quantity of crystallized zircons during diagenetic processes is not always abundant, but rather limited. In some cases, the thermochemical conditions may not fully support zircon crystallization. For instance, zircon crystallization is generally favored

in igneous rocks with SiO_2 contents greater than 60%, as opposed to those with lower silica contents [31]. There is likely no evidence of zircon grains or age components throughout an entire crustal cycle involving collision, accretion, heating and loading, melting, and ultimately denudation [32].

The tectonic setting also exerts a significant influence on the fertility and preservation of zircon through its impact on igneous rocks [18,32]. Within the convergent plate margin background, igneous rocks exhibit high productivity; however, their conservation potential is relatively low. Within the collisional setting, igneous rock formation is less productive and primarily results from partial melting of the crust. Nevertheless, their preservation potential is enhanced by supercontinent assembly. In extensional settings, there are significant variations in production rates with dominance of mafic rocks that have limited zircon fertility [32]. The ages of igneous rocks coinciding with supercontinental aggregation events may not necessarily indicate the primary stage of crustal formation, but rather reflect the favorable conditions for preserving these rocks in their environment [18]. In other words, the formation and preservation mechanism of zircons can introduce bias to detrital zircon age data, potentially leading to ambiguous or even untraceable recorded provenance information descriptive of geological processes [18,32,33].

The processes of uplift and denudation significantly impact the recording of provenance information by detrital zircons. As primary contributors to sedimentary rock formation, both protoliths and sedimentary rocks have the potential to undergo uplift and/or denudation. For extreme examples, if the crystalline basement is extensively covered by later sediments, the well-preserved basement may not provide clear provenance clues in subsequent strata due to insufficient denudation [20]. In contrast, intense denudation can remove parent rocks in provenance areas (e.g., unroofing), and some identified detrital zircon age components may not find suitable provenance under current topographic conditions or paleogeographic context [34]. Therefore, the geological evolution history should be collectively considered in provenance analysis.

Last but not least, lag time, which refers to the interval between zircon crystallization ages and sediment deposition ages, is another factor that may influence a provenance analysis [20]. Generally speaking, volcanic rocks with low zircon fertility exhibit shorter lag times [35], while intrusive rocks have relatively longer lag times depending on the depth of the intrusion invasion and the denudation rate of overlying rocks [6]. Furthermore, variations in lag time are closely associated with tectonic environments as well [31,36]. Within basins, at convergent margins, more than 50% of detrital zircons have crystallization ages close to stratigraphic ages. In basins formed in a collisional background, there are small amounts of detrital zircons with crystallization ages close to stratigraphic ages. In an extensional background setting, the lag time is generally large [31]. During practical analysis, age components that are not represented in the detrital zircon age spectrum cannot be ignored and should be discussed together with the tectonic background.

According to studies specialized in the bias of detrital zircon age data, causative factors have been widely recognized. Proper treatments for these factors were discussed and developed as new standards to facilitate provenance analysis [5]. In conjunction with advancements in quantitative methodologies, detrital zircon U-Pb geochronology has already established a robust logical framework. As a result, provenance information is now more reliable and indicative of source terrains [5]. These significant improvements will undoubtedly benefit current and future age data acquisition and interpretation. However, it should be noted that long-term accumulated age datasets constructed at different developmental stages of detrital zircon U-Pb geochronology remain an important source of provenance information despite being inherently biased. The extraction and integration of both new and existing age datasets to uncover novel insights are crucial topics for future provenance analyses. Therefore, additional efforts are required in the development and promotion of quantitative methods in detrital zircon geochronology.

3. Local Singularity Analysis

Within the context of complexity science, the Earth system is often regarded as inherently nonlinear, with typical manifestations including one cause leading to multiple effects or one effect being influenced by multiple causes [37,38]. Numerous quantitative approaches have been developed and employed to explore the nonlinear properties of the Earth system in order to better understand geological processes and their associated sub-processes in both spatial and temporal scenarios [39]. As mentioned above, detrital zircons preserved in sedimentary rocks are widely recognized as final products resulting from various nonlinear geological processes such as magmatism, crystallization, uplift and denudation, transport, and deposition. The processes from formation to deposition are often interconnected, interactive, and intercoupled; even small variations can have disproportionate impacts on the discovery of detrital zircons. U-Pb age data serve as fundamental observational information in detrital zircon geochronology [11] and can therefore be analyzed using nonlinear methodologies. By characterizing U-Pb age distributions on an age spectrum (Figure 1), we can gain insights not only into the nonlinearity of the forming–preservation process but also into the nonlinear nature of Earth's evolution recorded by detrital zircons.

In previous decades, Gaussian and power law distributions have been commonly used as distribution models to characterize peak-and-trough patterns on the age spectrum [16]. The former is suitable for samples or data that follow normal or log-normal distributions, while the latter can effectively describe geological phenomena in the form of extreme events, which are often considered outliers in the former [16]. Due to their stable physical–chemical properties, detrital zircons contain traceable information related to their source and are often mixed and influenced by multiple factors and processes [16,18,33]. As a result of the complex formation–preservation processes' nonlinearity inheritance, age data frequently exhibit heterogeneous distribution in both spatial and temporal scenarios. Provenance information recorded by detrital zircons is primarily associated with extreme events that should be handled with caution. To better characterize provenance information, local singularity analysis is currently employed to characterize power law distributions on the age spectrum.

As originally proposed, the local singularity analysis is a nonlinear method to investigate extreme geological events that occurred within short spatial–temporal intervals and were accompanied by associated irregular energy release or material accumulation. According to estimate power law relations between observational data, measurable physical quantities (ρ) caused by extreme events (e.g., phase transition, self-organized criticality, and multiplicative cascade processes) and observation scales (ε), spatial variations in physical–chemical signatures can be characterized by a singularity index (k), quantitatively and qualitatively. A general model of the local singularity analysis [16] can be expressed as:

$$\rho(\varepsilon_i) \propto c\varepsilon_i^{-k} \tag{3}$$

where c is a constant determining the magnitude of the functions. In order to estimate the singularity index, a log transformation can be taken on both sides of the power law model (Equation (3)):

$$log\rho(\varepsilon_i) \propto -klog\varepsilon_i \tag{4}$$

Plotting $\rho(\varepsilon_i)$ and their corresponding scales (ε_i), the singularity index k can consequently be estimated using the slope. The local singularity analysis has been extensively discussed in the field of mineral exploration, particularly when considering 2-dimensional geochemical data as an example. In this estimation process, applied to all locations within a study area, the spatial variation of physical quantities is represented by positive ($k > 0$) and negative singularities ($k < 0$), which, respectively, characterize accumulation and depletion phenomena [16].

When applying the local singularity analysis to detrital zircon U-Pb age data, a power law relationship between the two variables in the age spectrum (Figure 1) can be expressed:

$$\rho(\Delta t_i) \propto \frac{1}{\Delta t_i} N(\Delta t_i) \propto c\Delta {t_i}^{-k} \quad (5)$$

where $\rho(\Delta t_i)$ is the average number of ages within different time intervals Δt_i (unit in Ma). Similarly, the singularity index k is estimated using the slope on the logarithmic–logarithmic plot. By implementing this estimation at all chronological ages, a series of singularity indices k can be derived, which establishes a novel age spectrum based on nonlinearity, known as the singularity spectrum (Figure 2). A value of $k < 1$ indicates depletion of detrital grains and implies an inactive and calm period. Conversely, a value of $k > 1$ represents accumulation of detrital grains and suggests productive crystallization along with effective preservation of zircons due to intensive magmatic activities. Provenance information, which was previously weak and mixed as indicated by the age spectrum, is now separated and/or enhanced (Figure 1b) to rectify biases arising from nonlinearity of detrital zircon-related geo-processes (e.g., diversities in zircon fertility and preservation). This singularity-based graphic method allows for interpretation of variations in age population and subsequent correlation with their potential provenance more accurately.

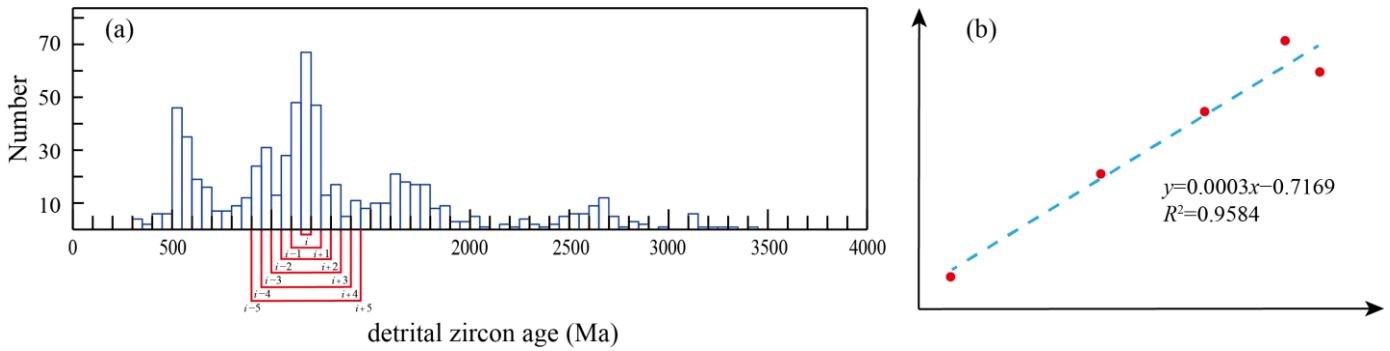

Figure 2. Schematic diagrams illustrating the application of the local singularity to an age spectrum (**a**) and the estimation process of singularity index k (**b**).

The local singularity theory was employed to quantitatively analyze five globally published zircon age datasets and presented a singularity age spectrum that effectively addressed concerns related to sampling and preservation [16]. By examining its correlation with significant geological events throughout the Earth's evolution, a descending trend observed in the singularity age spectrum was discussed. Furthermore, by comparing it with other time series data pertaining to mantle temperature, ocean sediment flux, and lithosphere thickening, a cooling model for mantle evolution was established, which predicted the cessation of plate tectonics at 1.45 Ga. Following this research, the local singularity analysis has been further utilized to investigate various significant issues related to geological evolution, crustal thickness, atmospheric oxygenation history, etc. [40–47]. The present study focuses on provenance analysis based on detrital zircon geochronological data and introduces a novel graphical method known as the local singularity spectrum. This method is practically applied in a case study exploring the connections between the Tibetan Plateau and Australia.

4. Case Study

4.1. Study Area

The Tibetan Plateau, being the largest plateau in the world, serves as a natural laboratory for investigating the geodynamic mechanisms of continent–continent collision zones [48–50]. Additionally, it provides an ideal location to validate theories of continental drift and plate tectonics. Its main components originated from the northern margin of

Gondwana, documenting the evolutionary history from microcontinental breakup and rift-drift to their eventual fit with the southern margin of the Asian continent [49,51–57]. According to long-term studies, the Tibetan Plateau, consisting of the Qiangtang (Northern and Southern), Lhasa, and Himalaya (Tethyan, High and Lesser) terranes (Figure 3), has been extensively investigated. A substantial amount of observational data has progressively accumulated, significantly enhancing our understanding of the tectonic evolution of the Tibetan Plateau during various geological periods.

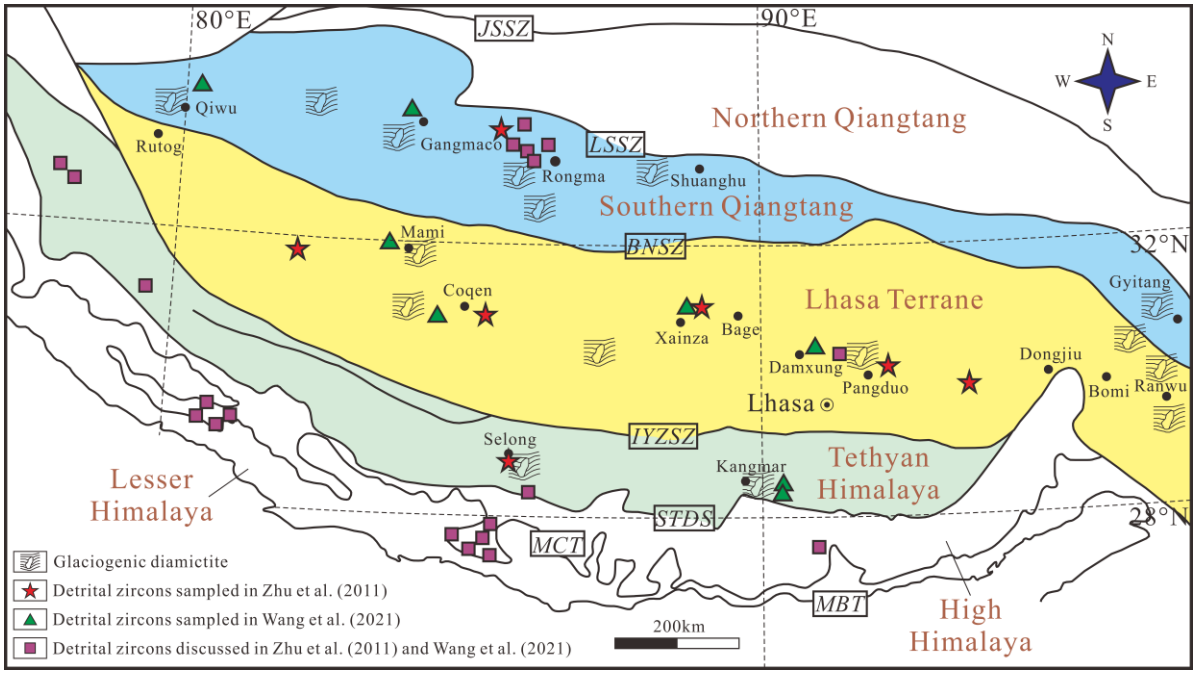

Figure 3. A simplified geological map of the Tibetan Plateau and sampling locations of detrital zircon samples (modified from [58,59]). **JSSZ**: Jinsha Suture Zone; **LSSZ**: Longmu Tso-Shuanghu Suture Zone; **BNSZ**: Bangong-Nujiang Suture Zone; **IYZSZ**: Indus-Yarlung Zangbo Suture Zone; **STDS**: Southern Tibetan Detachment System; **MCT**: Main Central Thrust; **MBT**: Main Boundary Thrust.

The origin of the Lhasa terrane has been extensively discussed in numerous studies focusing on two main viewpoints. The first viewpoint suggests an Indian Gondwana origin: prior to the Permo-Carboniferous period, the Lhasa terrane was positioned along the southern margin of Gondwana as a passive continental margin within the southern Paleo-Tethyan realm, alongside the Qiangtang, Indian, and Himalaya terranes. During the Mesozoic era, both the Qiangtang and Lhasa terranes separated from India Gondwana and gave rise to Meso-Tethys (e.g., Bangongco–Nujiang ophiolitic mélange belts) and Neo-Tethys (e.g., Yarlung Tsangpo ophiolitic mélange belts), respectively [48,49,56,57,60]. The second perspective supports the Australian origin of Gondwana: prior to the Permo-Carboniferous period, the Lhasa, Burma, Thailand, and Malaya terranes were located on the southern margin of Gondwana and constituted its passive continental margin in the southern Paleo-Tethyan region with Australia. During the Mesozoic era, these terranes separated from Australia Gondwana and formed Neo-Tethys (e.g., the Yarlung Tsangpo ophiolitic mélange belt) [51–53]. Among these studies, geological evidence is typically derived from the analysis of sedimentary facies, magmatic rocks, paleomagnetic data, Permo-Carboniferous glaciogenic diamictites (PCGDs), terrestrial plants, and tropical–subtropical marine fauna. Detrital zircon U-Pb ages are commonly used data in provenance analysis that play a fundamental role in understanding paleogeography and reconstructing the evolution of these main terranes and microcontinental fragments [8].

4.2. Datasets and Graphical Visualization

In order to investigate the origin of the Lhasa terrane, two sets of detrital zircon age data have been compiled [58,59], incorporating newly dated age data along with other published information from the regions of Southern Qiangtang, Lhasa, Tethyan Himalaya, and Western and Northern Australia terranes [36,61–69]. The origin and affinity of these terranes were discussed in these two studies through age spectrum correlation, leading to exciting results. In the current study, we further analyze these two datasets using a singularity spectrum within the context of provenance affinity.

The first dataset [58] primarily consists of detrital zircon U-Pb age data obtained using LA–ICPMS. It includes six Permo-Carboniferous metasedimentary rock samples from the Lhasa terrane, with a total of 547 analyses [58,61]. Additionally, it comprises nine Neoproterozoic quartzite and Cambrian–Permian sandstone samples from the Tethyan Himalaya terrane, with a total of 475 analyses [58,62,63]. Furthermore, it encompasses six Central Qiangtang metamorphic rock samples from the Southern Qiangtang terrane, with a total of 547 analyses [58,64,65]. Lastly, it incorporates eight Permian sandstone samples from the Southern Australia terrane, with a total of 475 analyses [36,68]. The age spectra of Lhasa and Western Australia exhibit prominent peaks at approximately 1170 Ma, as visualized in histograms with a bin width of 50 Ma and probability density plots (Figure 4a,d). In contrast, the age spectra of Southern Qiangtang and the Tethyan Himalaya demonstrate distinct peaks around 950 Ma (Figure 4b,c). These inconsistent age peaks between Lhasa (ca. 1170 Ma) and Southern Qiangtang–Tethyan Himalaya (ca. 950 Ma), as discussed previously [58] suggest that these Proterozoic detrital zircons originated from different provenances. Furthermore, the similarities observed among the age populations of Permo-Carboniferous metasedimentary rocks extensively distributed in Lhasa and Permian sandstones in Western Australia imply their common source regions due to the presence of widespread coeval magmatic rocks [58]. The former group exhibits a dominant peak at approximately 950 Ma but lacks one at around 1170 Ma, whereas the latter group displays a dominant peak at about 1170 Ma but lacks one at approximately 950 Ma. Based on these age spectra, the main terranes of the Tibetan Plateau can be classified into two groups: Southern Qiangtang–Tethyan Himalaya and Lhasa–Western Australia. These groups exhibit distinct spectrum characteristics that indicate different source regions. Based on the identical range of $\varepsilon_{Hf}(t)$ and corresponding peaks observed around 530 and 950 Ma (Figures 2a and 3a in Zhu et al., 2011 [58]), it was suggested that detrital zircons from the former group originated from similar source areas [66,67]. Regarding the second group, age spectra of Lhasa and Western Australia exhibit peaks at approximately ca. 1170 Ma with $\varepsilon_{Hf}(t)$ values ranging from −13.7 to +8.5 and −16.3 to +8.9, respectively [58]. In comparison to the geological history of Western Australia, extensively exposed coeval magmatic rocks were discovered in the Albany-Fraser belt [70], which have been reported as the primary source of the Collie and Perth Basins [19,36,71]. Along with the similarity observed in age spectra, these detrital zircons may originate from common resource regions within the Albany-Fraser belt in Western Australia [36,68], thereby supporting a geographical association between the Lhasa terrane and Australia during the late Precambrian–early Paleozoic.

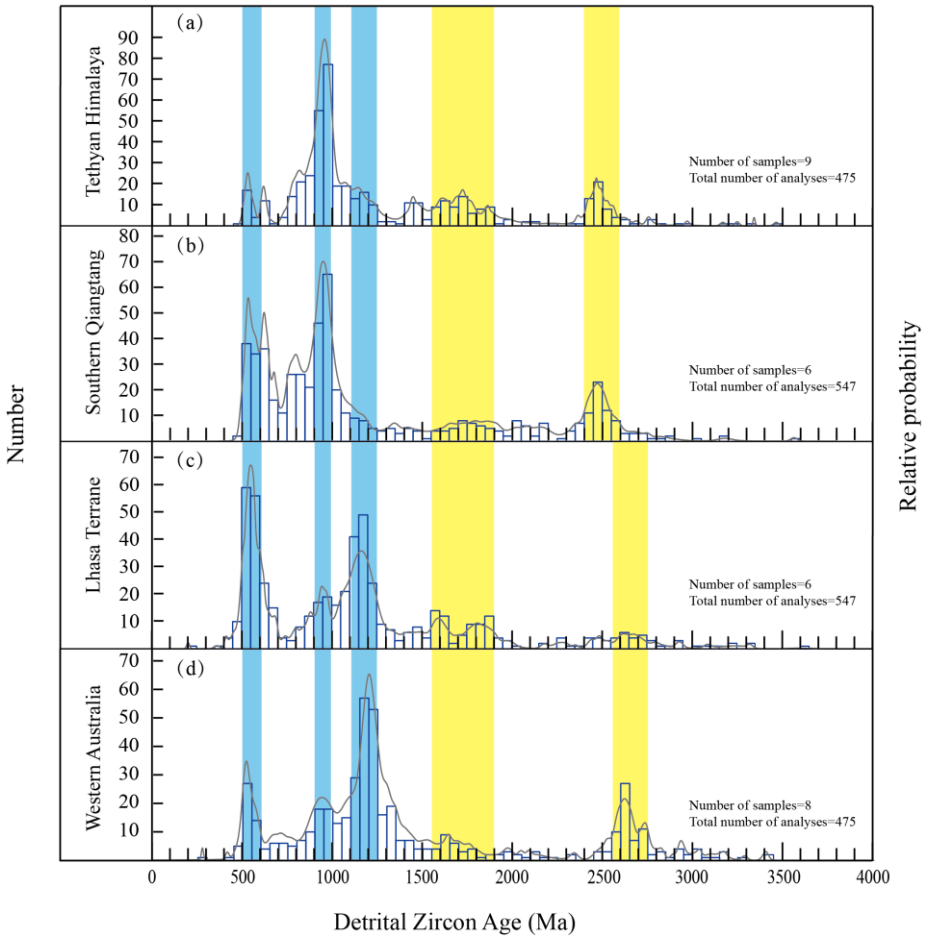

Figure 4. Detrital zircon U-Pb age spectra of the main terranes of the Tibetan Plateau reported in [58]. The blue transparent bands prominently highlight the characteristic age intervals that serve as the main focus in the original data, while the yellow transparent bands conspicuously indicate the supplementary age ranges discussed in this study.

The second dataset used in this follow-up study comprises detrital zircon U-Pb age data obtained using LA–ICPMS from the Tibetan Plateau and Australia. Samples collected from the Southern Qiangtang, Lhasa, and Tethyan Himalaya terranes (Figure 3) primarily consist of widespread Permo-Carboniferous glaciogenic diamictites (PCGDs), which are considered crucial carriers of provenance information for paleogeographic reconstruction of Gondwana-derived terranes [58,59]. The detrital zircons were primarily selected from matrices of pebbly slates and sandstones, as well as clasts of sandstones (Figure 5). The detrital zircon data from the Southern Qiangtang PCGDs consist of six matrix samples with a total of 560 analyses, along with one clast sample comprising 96 analyses. Similarly, the Lhasa PCGDs include eight matrix samples with a total of 689 analyses and four clast samples consisting of 329 analyses. Additionally, the Tethyan Himalaya PCGDs comprise two matrix samples with a total of 202 analyses and two clast samples containing a combined number of 189 analyses. Lastly, the Australian samples encompassed seven sandstone specimens from the Canning Basin in Northern Australia, which underwent analyses totaling 331 [69]. The age spectra of detrital zircons from PCGDs exhibit similar patterns, providing strong support for the conclusions drawn in the first dataset [58]. The spectra clearly demonstrate both similarities and differences, allowing for the classification of these four terranes into two distinct groups: Southern Qiangtang–Tethyan Himalaya and Lhasa–Northern Australia. However, the identification of several newly discovered peaks provides additional detailed provenance clues. In the case of the first group, the presence of similar peaks at approximately 820, 950, and 2480 Ma, along with corresponding $\varepsilon_{Hf}(t)$

values, supports a joint interpretation. Furthermore, comparison with orthogneisses from northern India dated to 820 Ma, Eastern Ghats–Rayner Provinces in southeastern India, and Dongargarh igneous rocks aged between 2432–2506 Ma in central India suggests that Southern Qiangtang and the Tethyan Himalaya likely originated from India Gondwana [59]. For the second group, the age spectra of Lhasa and Northern Australia exhibit similar age distributions with distinct peaks at approximately 1170 and 1760 Ma. This correlation is further supported by corresponding $\varepsilon_{Hf}(t)$ values, establishing a clear provenance connection between Lhasa and Australia [58,59]. By jointly comparing the $\varepsilon_{Hf}(t)$ values of detrital zircons from Lhasa with those of coeval detrital and magmatic zircons from Australia, it can be determined that the detrital zircons around 1170 Ma originated from basins in Western Australia [68,72], specifically the Albany-Fraser Orogen in Southwestern Australia and the Musgrave Orogen in Central Australia [73,74]. On the other hand, those around 1760 Ma are sourced from the Canning Basin as well as Albany-Fraser igneous rocks in Australia [59].

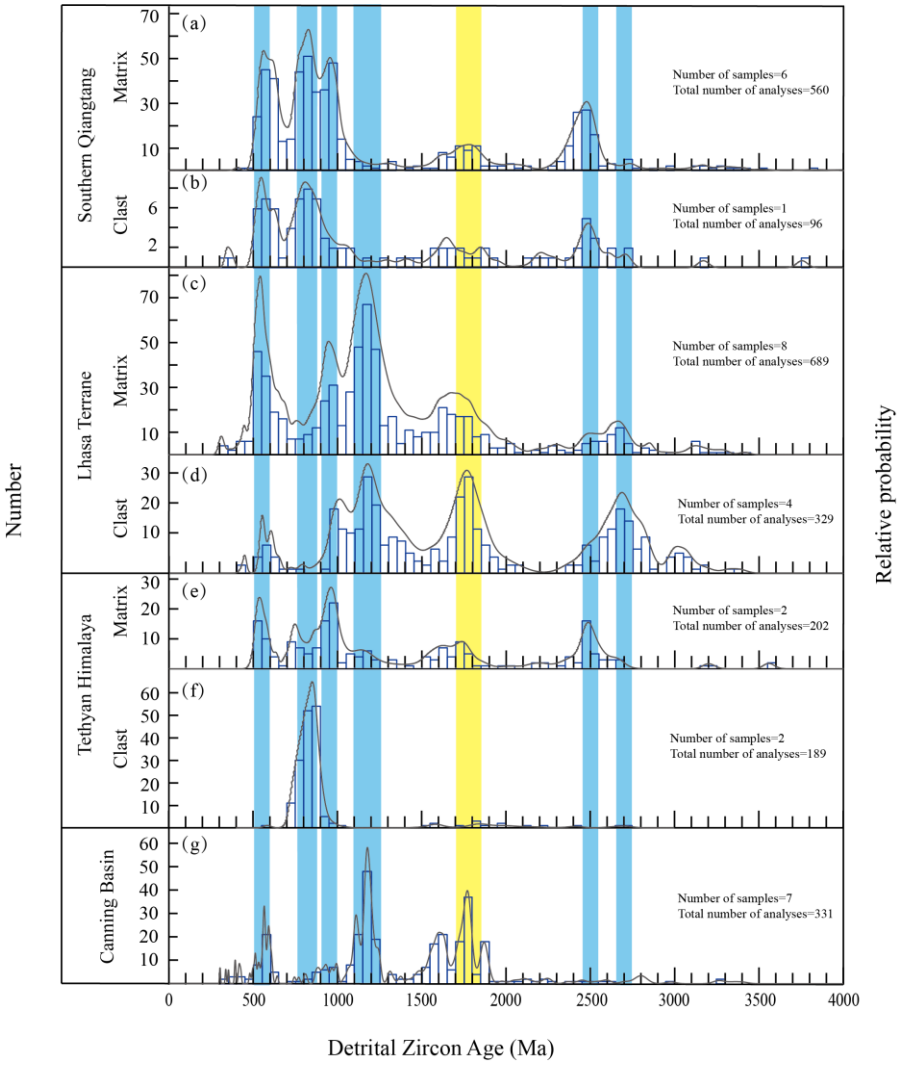

Figure 5. Detrital zircon U-Pb age spectra of the main terranes of the Tibetan Plateau reported in [59]. The blue transparent bands prominently highlight the characteristic age intervals that serve as the main focus in the original data, while the yellow transparent band conspicuously indicates the supplementary age range discussed in this study.

4.3. Singularity Analysis of U-Pb Age Data

The application of detrital zircon U-Pb geochronology in provenance analysis involves three main sequential steps or criteria, namely spectrum correlation, comparison of Hf isotopic data, and association with coeval magmatism/metamorphism. Firstly, the presence of similar age peaks among detrital zircons in sediments from different regions provides crucial evidence to narrow down the spatial–temporal ranges of potential resource areas. Secondly, a comparison and contrast of Hf isotopic data is conducted to ascertain whether the source magmas of these zircons exhibit comparable heterogeneity. Subsequently, an initial provenance link can be established between sediments displaying similar age peaks and exhibiting comparable Hf isotopic ranges. Lastly, coeval magmatism and/or metamorphism in potential resource areas serve as necessary evidence to validate the occurrence of zircon crystallization in these source regions. According to previous studies on provenance analysis, the paleogeographic constraints of the main terranes have provided supplementary evidence and/or clues for understanding the tectonic evolution of the Tibetan Plateau [58,59]. During the process of cognition, the affinity between the Lhasa and Australian terranes has been identified and supported by geochronological data. As depicted in spectral figures (Figures 4 and 5), a distinct age peak between 1600 and 1800 Ma is observed in the spectrum of the second dataset (Figure 5), whereas it appears weak and inconspicuous in the spectrum of the first dataset (Figure 4). Provenance links identified from these two datasets have progressively improved as previously weak information was enhanced and subsequently recognized in the second dataset. Consequently, utilizing provenance clues from this second dataset can facilitate steps such as Hf isotopic data comparison and establishing associations with coeval magmatism/metamorphism, ultimately leading to a clear and improved provenance link between the Lhasa and Australian terranes during 1600–1800 Ma.

The biases in detrital zircon age data, which lead to limited information or peaks on detrital zircon age spectra, are influenced by various factors associated with sampling, data analysis, and geological mechanisms. As widely acknowledged, the fertility and preservation potential of zircons vary across different tectonic settings [18]. Two currently discussed datasets obtained from diverse sedimentary media at multiple locations provide mutually complementary and corroborative evidence for provenance links that effectively demonstrate the heterogeneous distribution of preserved zircons in the Earth's crust. This also emphasizes why existing detrital zircon age data are crucial and should be integrated and jointly interpreted with new data to obtain a more comprehensive understanding of provenance. Detrital zircons and other minerals derived from diverse sedimentary sources have emerged as prominent focal points in geochronology-based provenance analysis. The primary objective of these endeavors is to capture the recorded provenance information that has been preserved within the Earth's crust. It is evident that when detrital zircon-bearing sediment samples are collected from appropriate sources with statistically stable quantities, the identified provenance information will become more informative and reliable. However, it remains foreseeable that zircons containing crucial information may potentially be lost or not preserved due to geological activities.

The enhancement of knowledge and experience in sampling and analysis is also a crucial criterion for maintaining the precision and accuracy of detrital zircon age data. The prominent peak observed between 1600 and 1800 Ma, which has been newly identified in the second dataset, suggests potential clues and/or weak information in the first dataset. The spectra (Figures 4 and 5) indicate that the average number of analyses conducted on each sedimentary sample (<100) in these two datasets is lower than the minimum quantity obtained from statistical studies on bias [19]. It should be noted that these average numbers (Figures 4 and 5) are not deemed inappropriate, as having 60 analyses per sample still adheres to a common criterion in geochronology [25,26]. However, based on statistical studies on bias, an amount less than 100 or 117 may introduce biases that could potentially result in compromised information [19]. Therefore, the integration of additional existing datasets should be emphasized to mitigate weak information to some extent. Furthermore,

it is crucial to consider that while strong information (or peaks) is enhanced, the weaker information may be further overshadowed. It becomes necessary to identify and thoroughly extract weak provenance information from these data in order to ensure the quality of new data. Numerous significant and informative provenance links recorded in existing detrital zircon data can consequently be fully utilized and integrated.

In order to enhance the weak information preserved in the original detrital zircon U-Pb age data, local singularity analysis is applied to these two datasets in the form of a histogram with a bin size of 50 Ma. Following the estimation process of a one-dimensional window-based method [16], the singularity index spectrum is currently established according to three steps. First and foremost, a series of 1D windows centered on the initial bin Δt_i are defined as $L_n(\sum_1^n \Delta t_i)$ (n = 6). Taking the example of the bin range from 300 to 350 Ma, this series includes $L_1(\Delta t_i)$, $L_2(\sum_{i-1}^{i+1} \Delta t_i)$, $L_3(\sum_{i-2}^{i+2} \Delta t_i)$, $L_4(\sum_{i-3}^{i+3} \Delta t_i)$, $L_5(\sum_{i-4}^{i+1} \Delta t_i)$, and $L_6(\sum_{i-5}^{i+5} \Delta t_i)$ (Figure 2) covering respective ranges of bins: 300–350 Ma, 250–400 Ma, 200–450 Ma, 150–500 Ma, 100–550 Ma, and 50–600 Ma. Secondly, by plotting the window sizes n and corresponding $\rho(\Delta ti)$ on a log–log graph, the slope of the linear relationship between window sizes n and the average number of ages within different windows $\rho(\Delta t_i)$ can be used to directly estimate the singularity index k at the initial bin Δt_i (i.e., 300–350 Ma) (Figure 2). Thirdly, implementing these two steps for all bins in both datasets will yield all singularity indices that subsequently create the corresponding singularity index spectra. The accompanying R^2 values for estimation at all bins can be depicted to evaluate whether these estimated singularity indices accurately characterize power law relations (Figures 6 and 7). In this study, the singularity index k infers accumulation or depletion of zircon grains when $k > 0$ or $k < 0$, respectively.

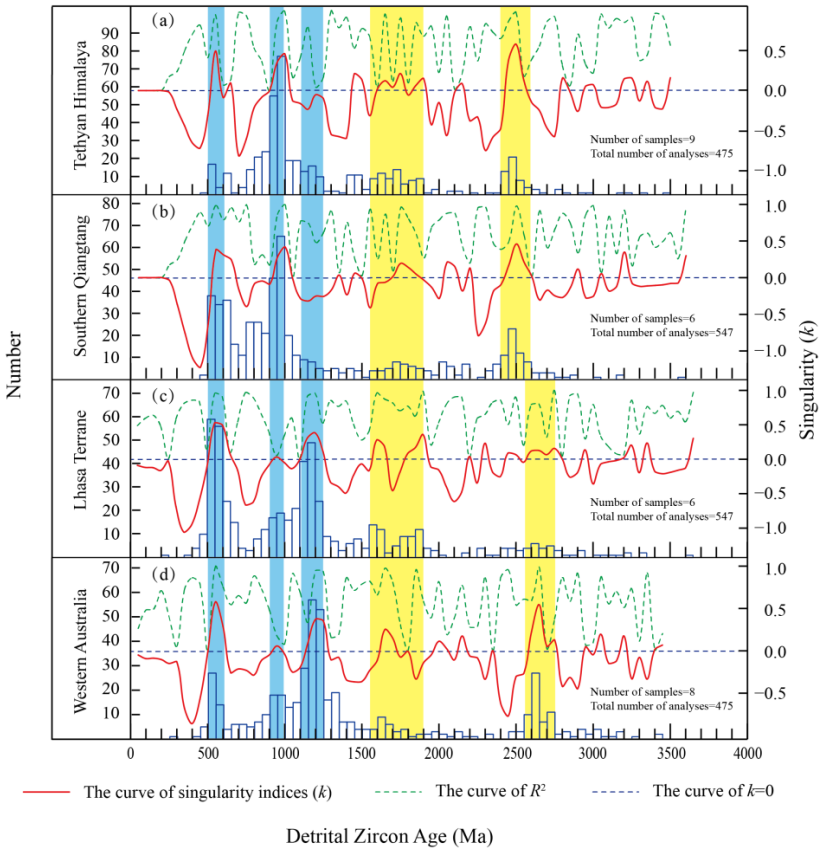

Figure 6. Singularity index spectra of detrital zircon U-Pb age data of the main terranes of the Tibetan Plateau reported in [58]. The blue transparent bands prominently highlight the characteristic age intervals that serve as the main focus in the original data, while the yellow transparent bands conspicuously indicate the supplementary age ranges identified in singularity spectra.

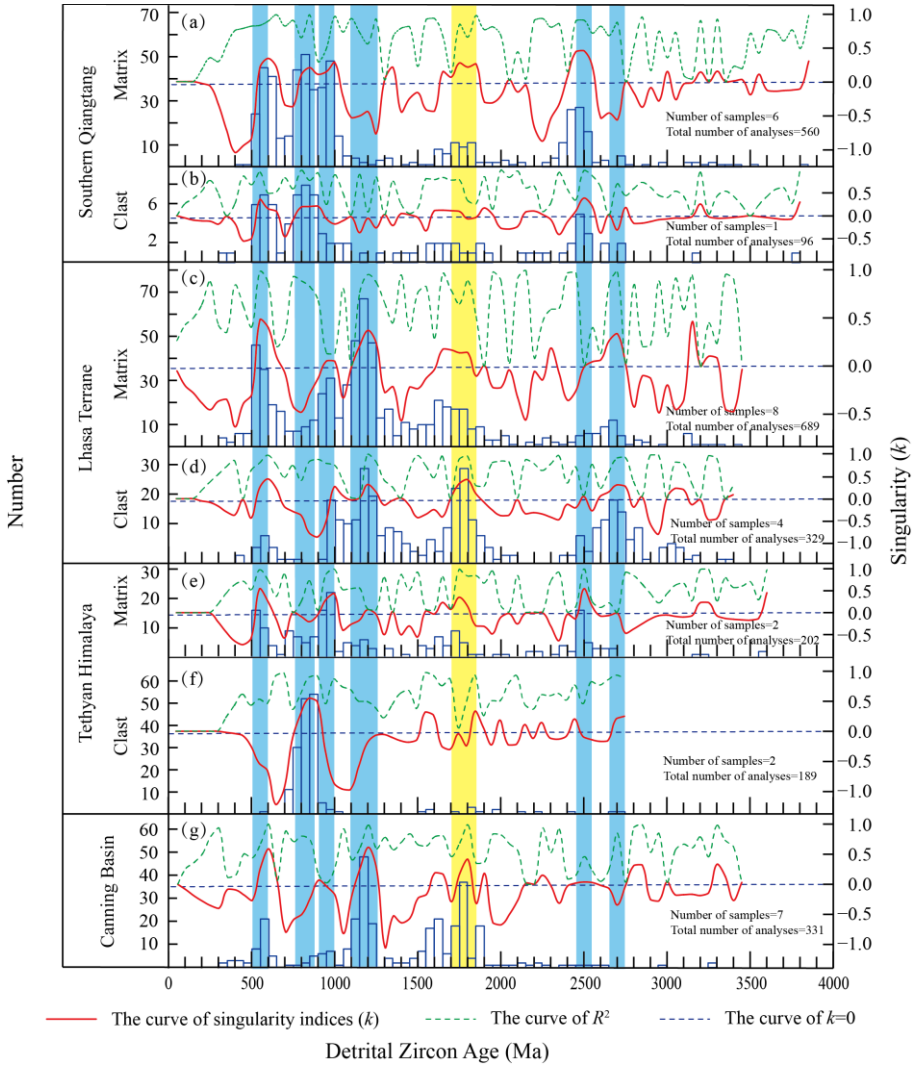

Figure 7. Singularity index spectra of detrital zircon U-Pb age data of the main terranes of the Tibetan Plateau reported in [59]. The blue transparent bands prominently highlight the characteristic age intervals that serve as the main focus in the original data, while the yellow transparent band conspicuously indicates the supplementary age range identified in singularity spectra.

The singularity spectrum of the first dataset (Figure 6) reveals that singularity peaks at approximately 530, 950, and 1170 Ma divide the four terranes into two distinct groups: Southern Qiangtang–Tethyan Himalaya and Lhasa–Western Australia. This observation is consistent with the findings from the age spectrum analysis (Figure 4), without any conflicting results. Furthermore, certain subtle peaks on the age spectrum (Figure 4) become more prominent in the singularity spectrum (Figure 6) due to the enhanced effect of local singularity analysis on weak provenance information. The singularity spectra of the Southern Qiangtang and Tethyan Himalaya exhibit clear similarities, as evidenced by the presence of newly identified dominant peaks at approximately 2500 Ma and subordinate peaks at around 1500 Ma. By evaluating their R^2 values, we selected the dominant peaks at ca. 2500 Ma, which show high R^2 values in both singularity spectra, as enhanced provenance information or clues revealed through local singularity analysis. Following the three criteria or steps of provenance analysis, we compare and contrast $\varepsilon_{Hf}(t)$ at ca. 2500 Ma from samples collected in these two terranes. Unfortunately, based on Hf isotopic data in the first dataset (Figure 8a), it is evident that the source magma for these detrital zircons does not match and lacks similar heterogeneity between them. The detrital zircons from Southern Qiangtang with an $\varepsilon_{Hf}(t)$ ranging from −13.7 to 5.9 indicate a mixed crustal and

mantle source magma, while those from the Tethyan Himalaya with an $\varepsilon_{Hf}(t)$ less than 0 suggest a crustal source magma (Figure 8a). Without supporting evidence from Hf isotopic data, the new dominant peak observed on the singularity index spectrum of the first dataset can only provide probable or potential provenance clues, although previous studies [59] have reported coeval magmatic and metamorphic activities in these two terranes as well as India to elucidate their provenance connection and affinity around 2500 Ma. One possible reason is the limited number of $\varepsilon_{Hf}(t)$ analyses available for the Tethyan Himalaya, as only four analyses are insufficient to adequately represent the heterogeneity of source magma. This may also explain why the peaks around 2500 Ma on the age spectrum (Figure 4) are not distinct and appear weak. In order to evaluate singularity peaks in Lhasa's and Western Australia's singularity index spectra, R^2 is used as a preliminary measure. The subordinate peaks at 1550–1800 Ma and 2550–2750 Ma on the age spectra (Figure 4) have now been enhanced and identified as distinctive dominant peaks, establishing their preliminary provenance connections during these periods. These clues provide additional information that cannot be obtained from the age spectra alone. For Hf isotopic data at 1550–1800 Ma, Lhasa exhibits an $\varepsilon_{Hf}(t)$ ranging from −6.97 to 9.63, while Western Australia ranges from −7.66 to 8.74; for Hf isotopic data at 2550–2750 Ma, Lhasa ranges from −10.78 to 2.88 and Western Australia ranges from −7.72 to 5.36. These similar heterogeneities in source magma between these two terranes (Figure 8b), along with reported coeval magmatism of Lhasa and Western Australia [59,75,76] consequently establish provenance connections. However, it should be noted that there is an imbalance in the numbers of $\varepsilon_{Hf}(t)$ for these two terranes, and more data may provide more stable evidence regarding their provenance connections.

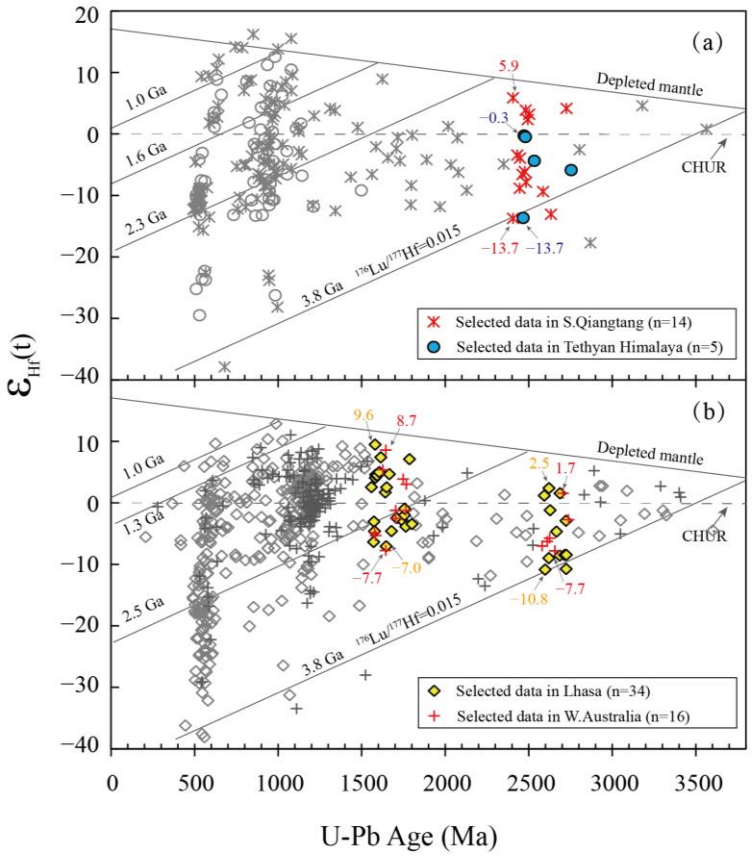

Figure 8. Plots of $\varepsilon_{Hf}(t)$ and detrital age data from Southern Qiangtang and the Tethyan Himalaya (**a**), as well as Lhasa and Western Australia (**b**), as reported in [58]. The highlighted colors indicate the periods discussed in the current study.

The application of local singularity analysis to the first dataset enhances weak provenance information on the age spectrum by quantitatively characterizing temporal variations in detrital zircon age populations. These preliminary provenance clues, which may be overlooked due to their inconspicuous expression, deserve attention. Furthermore, supported by the age spectra of the second dataset, the provenance affinity between Qiangtang–Tethyan Himalaya (ca. 2500 Ma) and Lhasa–Western Australia (ca. 1600 Ma) can be clarified, echoing established provenance connections identified in the singularity spectrum (Figures 6 and 7). To further explore practical applications of local singularity analysis in more detail, we analyze the second dataset to determine if any potential provenance clues have been overlooked in the age spectrum. From the singularity spectra of the second dataset (Figure 7), a similar grouping scheme can be established based on dominant singularity peaks, as mentioned above. For the Southern Qiangtang–Tethyan Himalaya group, peaks at approximately 820, 950, and 2480 Ma are retained with high R^2 values, without any new discoveries at other ages. The Lhasa–Australia group exhibits distinctive peaks at around 1170 and 1760 Ma. In the Lhasa spectrum, there is an enhancement of peaks in the range of 2650–2760 Ma; however, no corresponding peaks are observed in the Australia spectrum. These findings further demonstrate that local singularity analysis is an effective method for enhancing weak provenance information. By ensuring consistent provenance clues with those obtained from age spectra analysis, this method can provide additional clues to establish provenance connections even with a limited number of analyses, and offer preliminary guidance for future research endeavors. Moreover, it also emphasizes that both quantity of analyses and sampling coverage are crucial factors since well-preserved provenance information and a sufficient number of analyses serve as essential foundations for enhancing and recognizing weak provenance information.

The most significant advantage reflected in the current case study is to identify weak provenance information assisting in understanding the affinity of Southern Qiangtang–Tethyan Himalaya and Lhasa–Western Australia ca. 2500 and 1600 Ma, respectively (Figure 6). The identification was not clarified based on the first dataset due to weak information and limited quantity issues. Changing sampling media of detrital zircons (matrix and clast of PCGDS), more delicate analyses can then establish the affinity between these terranes ca. 1600 and 2500 Ma. Therefore, the current case study well demonstrates a new graphical method for age correlation for provenance analysis which can reveal more comprehensive and detailed provenance clues. Moreover, it facilitates making a strategy if more sampling and analyses are necessary to further enhance understanding of provenance in future work. Meanwhile, methods to quantify differences and similarities among age spectra can be considered for the correlation of singularity index spectra in the future. It should be expectable that singularity spectrum-based provenance analysis is not only effective in quantifying temporal variation in detrital zircon age population but also in improving missing and omission issues of weak but significant information.

5. Summary and Discussion

The utilization of detrital zircon U-Pb age as crucial geochronological data in provenance analysis is widespread. In the current era, effectively managing and fully exploiting long-term accumulated "big data" to gain a better understanding of geological evolution has become increasingly important. Within this context, the current study firstly reviews several causative factors that may introduce bias into the age population. A case study focusing on the affinity of the main terranes in the Tibetan Plateau is presented, utilizing two published datasets of detrital zircon ages. As described in the original literature, there is a noticeable progressive improvement in the understanding of provenance connections among these terranes through the analysis of detrital zircon age spectra obtained from various sources. Consequently, this study addresses issues related to unclear and weak provenance information preserved within the age data and practically applies local singularity analysis to both datasets. The new graphical approach effectively quantifies temporal variations in detrital zircon age populations and enhances the identification of weak prove-

nance information that may not be apparent on conventional age spectra. In particular, dominant singularity peaks reveal previously inconspicuous weak provenance signals, especially in the first dataset published over 10 years ago. Comparing these results with those from the second dataset reported within the last few years confirms established provenance connections identified through singularity spectra analysis. This graphical approach contributes a novel method for interpreting and comparing detrital zircon age spectra.

Enhanced weak information in singularity spectra provides new evidence for establishing preliminary provenance clues regarding the affinity between Lhasa and Australia or Southern Qiangtang and the Tethyan Himalaya. While the singularity spectrum effectively characterizes weak provenance information, supporting the establishment of provenance connections among the main terranes of the Tibetan Plateau, manipulating and fully exploiting both existing and future detrital zircon age data present ongoing challenges. Several concerns regarding future research are currently being explored.

In subsequent research, it is imperative to conduct comprehensive case studies that delve into the singularity spectrum through in-depth discussions and explorations. It is anticipated that a more extensive utilization of both conventional age spectra and singularity spectra will unveil additional provenance information. As observed in this study, the initial evidence supporting preliminary provenance links between Southern Qiangtang and the Tethyan Himalaya around 2500 Ma cannot be strongly substantiated due to the limited quantity of Hf isotopic data in the first dataset. This raises a new question: how many Hf isotopic values are required to adequately express the heterogeneity of source magma? The integration of self-collected samples with existing age data is likely to become a standard practice in numerous reported case studies. In future research, an extensive collection from open sources will enable the selection and analysis of more zircon grains within each self-collected sample, ensuring that recorded provenance information is accurately reflected through detrital zircon age data. Meanwhile, it is also suggested that the singularity spectrum can be utilized as a supplementary or reference to the conventional age spectrum in order to prevent omission and loss of weak provenance information. Therefore, future application of the singularity spectrum should incorporate both the R^2 value and singularity index for an optimized interpretation of singularity peaks and provenance clues. Consequently, the comparison of Hf isotopic data and association with coeval magmatism/metamorphism can be based on a stable and rational foundation.

Secondly, analytical methods for geochronological data primarily excel in identifying preserved provenance information but cannot replace the importance of systematic sampling and meticulous laboratory analyses (e.g., selection criteria for sampling media and grains). Similarly, a collection of detrital zircon age data established based on carefully chosen grains with an optimal number of analyses may still encounter issues related to bias and/or weak provenance information that necessitate further discussion through additional case studies. The present study acknowledges that weak provenance might be inevitable even when the data are analyzed following an optimal manipulation. The cause of weak information often lies in the formation and preservation mechanisms of detrital zircons, while biases caused by analytical errors or sampling strategies can be effectively rectified using advanced methods such as the singularity spectrum currently proposed. Therefore, it is essential to accept that certain objective provenance connections may not be preserved and recorded by detrital zircons alone. Greater attention may be paid to other mineral carriers like apatite for obtaining more comprehensive insights. Naturally, these discussions remain speculative prospects; definitive conclusions and knowledge will require further extensive research efforts in future studies.

Author Contributions: Conceptualization, W.W. (Wenlei Wang) and Y.P.; methodology, W.W. (Wenlei Wang) and Q.C.; software, W.W. (Wenlei Wang) and W.W. (Wenjun Wang); validation, W.W. (Wenlei Wang), Y.P., and W.W. (Wenjun Wang); formal analysis, W.W. (Wenlei Wang) and Q.C.; investigation, W.W. (Wenlei Wang) and Q.C.; resources, W.W. (Wenlei Wang); data curation, W.W. (Wenlei Wang) and Y.P.; writing—original draft preparation, W.W. (Wenlei Wang); writing—review and editing, W.W. (Wenlei Wang) and Y.P.; visualization, W.W. (Wenlei Wang), Y.P., and W.W. (Wenjun Wang); supervision, W.W. (Wenlei Wang); project administration, W.W. (Wenlei Wang); funding acquisition, W.W. (Wenlei Wang). All authors have read and agreed to the published version of the manuscript.

Funding: This research was jointly funded by the National Key Research and Development Program of China, grant number 2021YFC2901905, and the National Natural Science Foundation of China (41822206, 41772353).

Data Availability Statement: The data utilized in this study were collected from two published studies [59,60]. The first one can be downloaded from the GSA Data Repository item 2011221, which is available online at www.geosociety.org/pubs/ft2011.htm (https://doi.org/10.1130/2011221). The second one was found on the website https://osf.io/szk2q/ (https://doi.org/10.17605/osf.io/szk2q). All these data were accessed on 20 February 2022.

Acknowledgments: The authors would like to extend their sincere gratitude to guest editors for their invaluable efforts in organizing this special issue. Additionally, we would like to express our appreciation to the graduate students Changjiang Yuan and Jie Tang for their valuable assistance in preparing the manuscript.

Conflicts of Interest: Author Wenjun Wang was employed by the company Henan Fourth Geological Exploration Institute Co., Ltd. The remaining authors declare that the research was conducted in the absence of any commercial or financial relationships that could be construed as a potential conflict of interest.

References

1. Blatt, H.; Jones, R.L. Proportions of Exposed Igneous, Metamorphic, and Sedimentary Rocks. *GSA Bull.* **1975**, *86*, 1085–1088. [CrossRef]
2. Link, P.K.; Fanning, C.M.; Beranek, L.P. Reliability and Longitudinal Change of Detrital-Zircon Age Spectra in the Snake River System, Idaho and Wyoming: An Example of Reproducing the Bumpy Barcode. *Sediment. Geol.* **2005**, *182*, 101–142. [CrossRef]
3. Thomas, W.A.; Becker, T.P.; Samson, S.D.; Hamilton, M.A. Detrital Zircon Evidence of a Recycled Orogenic Foreland Provenance for Alleghanian Clastic-wedge Sandstones. *J. Geol.* **2004**, *112*, 23–37. [CrossRef]
4. Dickinson, W.R.; Gehrels, G.E. Use of U-Pb Ages of Detrital Zircons to Infer Maximum Depositional Ages of Strata: A Test against a Colorado Plateau Mesozoic Database. *Earth Planet. Sci. Lett.* **2009**, *288*, 115–125. [CrossRef]
5. Weltje, G.J.; von Eynatten, H. Quantitative Provenance Analysis of Sediments: Review and Outlook. *Sediment. Geol.* **2004**, *171*, 1–11. [CrossRef]
6. Gehrels, G.E.; Blakey, R.; Karlstrom, K.E.; Timmons, J.M.; Dickinson, B.; Pecha, M. Detrital Zircon U-Pb Geochronology of Paleozoic Strata in the Grand Canyon, Arizona. *Lithosphere* **2011**, *3*, 183–200. [CrossRef]
7. Scherer, E.E.; Whitehouse, M.J.; Münker, C. Zircon as a Monitor of Crustal Growth. *Elements* **2007**, *3*, 19–24. [CrossRef]
8. Gehrels, G. Detrital Zircon U-Pb Geochronology: Current Methods and New Opportunities. In *Tectonics of Sedimentary Basins*; John Wiley & Sons, Ltd.: Hoboken, NJ, USA, 2011; pp. 45–62, ISBN 978-1-4443-4716-6.
9. Finch, M.A.; Weinberg, R.F.; Barrote, V.R.; Cawood, P.A. Hf Isotopic Ratios in Zircon Reveal Processes of Anatexis and Pluton Construction. *Earth Planet. Sci. Lett.* **2021**, *576*, 117215. [CrossRef]
10. Fasulo, C.R.; Ridgway, K.D. Detrital Zircon Geochronology of Modern River Sediment in South-Central Alaska: Provenance, Magmatic, and Tectonic Insights into the Mesozoic and Cenozoic Development of the Southern Alaska Convergent Margin. *Geosphere* **2021**, *17*, 1248–1267. [CrossRef]
11. Puetz, S.J.; Ganade, C.E.; Zimmermann, U.; Borchardt, G. Statistical Analyses of Global U-Pb Database 2017. *Geosci. Front.* **2018**, *9*, 121–145. [CrossRef]
12. Amidon, W.H.; Burbank, D.W.; Gehrels, G.E. Construction of Detrital Mineral Populations: Insights from Mixing of U-Pb Zircon Ages in Himalayan Rivers. *Basin Res.* **2005**, *17*, 463–485. [CrossRef]
13. Jacobson, C.E.; Grove, M.; Pedrick, J.N.; Barth, A.P.; Marsaglia, K.M.; Gehrels, G.E.; Nourse, J.A. Late Cretaceous–Early Cenozoic Tectonic Evolution of the Southern California Margin Inferred from Provenance of Trench and Forearc Sediments. *GSA Bull.* **2011**, *123*, 485–506. [CrossRef]
14. Zhang, Z.M.; Schertl, H.-P.; Wang, J.L.; Shen, K.; Liou, J.G. Source of Coesite Inclusions within Inherited Magmatic Zircon from Sulu UHP Rocks, Eastern China, and Their Bearing for Fluid–Rock Interaction and SHRIMP Dating. *J. Metamorph. Geol.* **2009**, *27*, 317–333. [CrossRef]
15. Wernicke, B. The California River and Its Role in Carving Grand Canyon. *GSA Bull.* **2011**, *123*, 1288–1316. [CrossRef]

16. Cheng, Q.M. Singularity Analysis of Global Zircon U-Pb Age Series and Implication of Continental Crust Evolution. *Gondwana Res.* **2017**, *51*, 51–63. [CrossRef]
17. Parman, S.W. Helium Isotopic Evidence for Episodic Mantle Melting and Crustal Growth. *Nature* **2007**, *446*, 900–903. [CrossRef]
18. Hawkesworth, C.; Cawood, P.; Kemp, T.; Storey, C.; Dhuime, B. A Matter of Preservation. *Science* **2009**, *323*, 49–50. [CrossRef] [PubMed]
19. Vermeesch, P. How Many Grains Are Needed for a Provenance Study? *Earth Planet. Sci. Lett.* **2004**, *224*, 441–451. [CrossRef]
20. Thomas, W.A. Detrital-Zircon Geochronology and Sedimentary Provenance. *Lithosphere* **2011**, *3*, 304–308. [CrossRef]
21. Sircombe, K.N. Quantitative Comparison of Large Sets of Geochronological Data Using Multivariate Analysis: A Provenance Study Example from Australia. *Geochim. Cosmochim. Acta* **2000**, *64*, 1593–1616. [CrossRef]
22. Hietpas, J.; Samson, S.; Moecher, D.; Chakraborty, S. Enhancing Tectonic and Provenance Information from Detrital Zircon Studies: Assessing Terrane-Scale Sampling and Grain-Scale Characterization. *J. Geol. Soc.* **2011**, *168*, 309–318. [CrossRef]
23. Zimmermann, U.; Andersen, T.; Madland, M.V.; Larsen, I.S. The Role of U-Pb Ages of Detrital Zircons in Sedimentology—An Alarming Case Study for the Impact of Sampling for Provenance Interpretation. *Sediment. Geol.* **2015**, *320*, 38–50. [CrossRef]
24. Lawrence, R.L.; Cox, R.; Mapes, R.W.; Coleman, D.S. Hydrodynamic Fractionation of Zircon Age Populations. *GSA Bull.* **2011**, *123*, 295–305. [CrossRef]
25. Dodson, M.H.; Compston, W.; Williams, I.S.; Wilson, J.F. A Search for Ancient Detrital Zircons in Zimbabwean Sediments. *J. Geol. Soc.* **1988**, *145*, 977–983. [CrossRef]
26. Andersen, T. Correction of Common Lead in U-Pb Analyses That Do Not Report 204 Pb. *Chem. Geol.* **2002**, *192*, 59–79. [CrossRef]
27. Tucker, R.T.; Roberts, E.M.; Hu, Y.; Kemp, A.I.S.; Salisbury, S.W. Detrital Zircon Age Constraints for the Winton Formation, Queensland: Contextualizing Australia's Late Cretaceous Dinosaur Faunas. *Gondwana Res.* **2013**, *24*, 767–779. [CrossRef]
28. Schaltegger, U.; Schmitt, A.K.; Horstwood, M.S.A. U-Th-Pb Zircon Geochronology by ID-TIMS, SIMS, and Laser Ablation ICP-MS: Recipes, Interpretations, and Opportunities. *Chem. Geol.* **2015**, *402*, 89–110. [CrossRef]
29. Andersen, T.; Kristoffersen, M.; Elburg, M.A. Visualizing, Interpreting and Comparing Detrital Zircon Age and Hf Isotope Data in Basin Analysis—A Graphical Approach. *Basin Res.* **2018**, *30*, 132–147. [CrossRef]
30. Sircombe, K.N.; Hazelton, M.L. Comparison of Detrital Zircon Age Distributions by Kernel Functional Estimation. *Sediment. Geol.* **2004**, *171*, 91–111. [CrossRef]
31. Cawood, P.A.; Hawkesworth, C.J.; Dhuime, B. Detrital Zircon Record and Tectonic Setting. *Geology* **2012**, *40*, 875–878. [CrossRef]
32. Moecher, D.P.; Samson, S.D. Differential Zircon Fertility of Source Terranes and Natural Bias in the Detrital Zircon Record: Implications for Sedimentary Provenance Analysis. *Earth Planet. Sci. Lett.* **2006**, *247*, 252–266. [CrossRef]
33. Condie, K.C.; Arndt, N.; Davaille, A.; Puetz, S.J. Zircon Age Peaks: Production or Preservation of Continental Crust? *Geosphere* **2017**, *13*, 227–234. [CrossRef]
34. Stewart, J.H.; Gehrels, G.E.; Barth, A.P.; Link, P.K.; Christie-Blick, N.; Wrucke, C.T. Detrital Zircon Provenance of Mesoproterozoic to Cambrian Arenites in the Western United States and Northwestern Mexico. *GSA Bull.* **2001**, *113*, 1343–1356. [CrossRef]
35. Dickinson, W.R. Impact of Differential Zircon Fertility of Granitoid Basement Rocks in North America on Age Populations of Detrital Zircons and Implications for Granite Petrogenesis. *Earth Planet. Sci. Lett.* **2008**, *275*, 80–92. [CrossRef]
36. Cawood, P.A.; Nemchin, A.A. Provenance Record of a Rift Basin: U/Pb Ages of Detrital Zircons from the Perth Basin, Western Australia. *Sediment. Geol.* **2000**, *134*, 209–234. [CrossRef]
37. Wang, W.L.; Zhao, J.; Cheng, Q.M. Nonlinearity. In *Encyclopedia of Mathematical Geosciences*; Daya Sagar, B.S., Cheng, Q.M., McKinley, J., Agterberg, F., Eds.; Encyclopedia of Earth Sciences Series; Springer International Publishing: Cham, Switzerland, 2021; pp. 1–6. ISBN 978-3-030-26050-7.
38. Flinders, J.; Clemens, J.D. Non-Linear Dynamics, Chaos, Complexity and Enclaves in Granitoid Magmas. *Earth Environ. Sci. Trans. R. Soc. Edinb.* **1996**, *87*, 217–223. [CrossRef]
39. Ghil, M. A Century of Nonlinearity in the Geosciences. *Earth Space Sci.* **2019**, *6*, 1007–1042. [CrossRef]
40. Zhu, P.P.; Cheng, Q.M. Singularity Analysis of Volcanic Ages and Implications for Tectonic Setting in the Mesozoic, Great Xing'an Range, Northeast China. *Minerals* **2019**, *9*, 419. [CrossRef]
41. Zhou, Y.Z.; Cheng, Q.M.; Liu, Y.; Zhu, P.P.; Wu, G.P.; Zhang, Z.J.; Yang, J. Singularity Analysis of Igneous Zircon U-Pb Age and Hf Isotopic Record in the Zhongdian Arc, Northwest Yunnan, China: Implications for Indosinian Magmatic Flare-up and the Formation of Porphyry Copper Deposits. *Ore Geol. Rev.* **2021**, *139*, 104476. [CrossRef]
42. Zhang, Z.J.; Kusky, T.; Yang, X.K.; Cheng, Q.M. A Paradigm Shift in Precambrian Research Driven by Big Data. *Precambrian Res.* **2023**, *399*, 107235. [CrossRef]
43. Zhang, Z.J.; Kusky, T.; Gao, M.; Cheng, Q.M. Spatio-Temporal Analysis of Big Data Sets of Detrital Zircon U-Pb Geochronology and Hf Isotope Data: Tests of Tectonic Models for the Precambrian Evolution of the North China Craton. *Earth-Sci. Rev.* **2023**, *239*, 104372. [CrossRef]
44. Cheng, Q.M. Singularity Analysis of Magmatic Flare-Ups Caused by India—Asia Collisions. *J. Geochem. Explor.* **2018**, *189*, 25–31. [CrossRef]
45. Cheng, Q.M. Extrapolations of Secular Trends in Magmatic Intensity and Mantle Cooling: Implications for Future Evolution of Plate Tectonics. *Gondwana Res.* **2018**, *63*, 268–273. [CrossRef]
46. Chen, G.X.; Kusky, T.; Luo, L.; Li, Q.K.; Cheng, Q.M. Hadean Tectonics: Insights from Machine Learning. *Geology* **2023**, *51*, 718–722. [CrossRef]

47. Chen, G.X.; Cheng, Q.M.; Lyons, T.W.; Shen, J.; Agterberg, F.; Huang, N.; Zhao, M.L. Reconstructing Earth's Atmospheric Oxygenation History Using Machine Learning. *Nat. Commun.* **2022**, *13*, 5862. [CrossRef]
48. Allégre, C.J.; Courtillot, V.; Tapponnier, P.; Hirn, A.; Mattauer, M.; Coulon, C.; Jaeger, J.J.; Achache, J.; Schärer, U.; Marcoux, J.; et al. Structure and Evolution of the Himalaya–Tibet Orogenic Belt. *Nature* **1984**, *307*, 17–22. [CrossRef]
49. Yin, A.; Harrison, T.M. Geologic Evolution of the Himalayan-Tibetan Orogen. *Annu. Rev. Earth Planet. Sci.* **2000**, *28*, 211–280. [CrossRef]
50. Xu, Z.Q.; Ji, S.C.; Cai, Z.H.; Zeng, L.S.; Geng, Q.R.; Cao, H. Kinematics and Dynamics of the Namche Barwa Syntaxis, Eastern Himalaya: Constraints from Deformation, Fabrics and Geochronology. *Gondwana Res.* **2012**, *21*, 19–36. [CrossRef]
51. Audley-Charles, M.G. Reconstruction of Eastern Gondwanaland. *Nature* **1983**, *306*, 48–50. [CrossRef]
52. Audley-Charles, M.G. Cold Gondwana, Warm Tethys and the Tibetan Lhasa Block. *Nature* **1984**, *310*, 165. [CrossRef]
53. Audley-Charles, M.G. Evolution of the Southern Margin of Tethys (North Australian Region) from Early Permian to Late Cretaceous. *Geol. Soc. Lond. Spec. Publ.* **1988**, *37*, 79–100. [CrossRef]
54. Metcalfe, I. Late Palaeozoic and Mesozoic Tectonic and Palaeogeographical Evolution of SE Asia. *Geol. Soc. Lond. Spec. Publ.* **2009**, *315*, 7–23. [CrossRef]
55. Zhu, D.C.; Zhao, Z.D.; Niu, Y.L.; Mo, X.X.; Chung, S.L.; Hou, Z.Q.; Wang, L.Q.; Wu, F.Y. The Lhasa Terrane: Record of a Microcontinent and Its Histories of Drift and Growth. *Earth Planet. Sci. Lett.* **2011**, *301*, 241–255. [CrossRef]
56. Sengör, A.M.C. Tectonics of the Tethysides: Orogenic Collage Development in a Collisional Setting. *Annu. Rev. Earth Planet. Sci.* **1987**, *15*, 213–244. [CrossRef]
57. Sengör, A.M.C.; Cin, A.; Rowley, D.B.; Nie, S.Y. Space-Time Patterns of Magmatism along the Tethysides: A Preliminary Study. *J. Geol.* **1993**, *101*, 51–84. [CrossRef]
58. Zhu, D.C.; Zhao, Z.D.; Niu, Y.L.; Dilek, Y.; Mo, X.X. Lhasa Terrane in Southern Tibet Came from Australia. *Geology* **2011**, *39*, 727–730. [CrossRef]
59. Wang, Q.; Zhu, D.C.; Cawood, P.A.; Chung, S.L.; Zhao, Z.D. Resolving the Paleogeographic Puzzle of the Lhasa Terrane in Southern Tibet. *Geophys. Res. Lett.* **2021**, *48*, e2021GL094236. [CrossRef]
60. Sengör, A.M.C.; Atayman, S. The Permian Extinction and the Tethys: An Exercise in Global Geology. In *The Permian Extinction and the Tethys: An Exercise in Global Geology*; Sengör, A.M.C., Atayman, S., Eds.; Geological Society of America: Boulder, CO, USA, 2009; Volume 448, ISBN 978-0-8137-2448-5.
61. Leier, A.L.; Kapp, P.; Gehrels, G.E.; DeCelles, P.G. Detrital Zircon Geochronology of Carboniferous–Cretaceous Strata in the Lhasa Terrane, Southern Tibet. *Basin Res.* **2007**, *19*, 361–378. [CrossRef]
62. Myrow, P.M.; Hughes, N.C.; Goodge, J.W.; Fanning, C.M.; Williams, I.S.; Peng, S.; Bhargava, O.N.; Parcha, S.K.; Pogue, K.R. Extraordinary Transport and Mixing of Sediment across Himalayan Central Gondwana during the Cambrian–Ordovician. *GSA Bull.* **2010**, *122*, 1660–1670. [CrossRef]
63. Myrow, P.M.; Hughes, N.C.; Searle, M.P.; Almeida, C.M.; Peng, S.C.; Parcha, S.K. Stratigraphic Correlation of Cambrian–Ordovician Deposits along the Himalaya: Implications for the Age and Nature of Rocks in the Mount Everest Region. *GSA Bull.* **2009**, *121*, 323–332. [CrossRef]
64. Dong, C.Y.; Li, C.; Wan, Y.S.; Wang, W.; Wu, Y.W.; Xie, H.Q.; Liu, D.Y. Detrital Zircon Age Model of Ordovician Wenquan Quartzite South of Lungmuco-Shuanghu Suture in the Qiangtang Area, Tibet: Constraint on Tectonic Affinity and Source Regions. *Sci. China Earth Sci.* **2011**, *54*, 1034–1042. [CrossRef]
65. Pullen, A.; Kapp, P.; Gehrels, G.E.; Vervoort, J.D.; Ding, L. Triassic Continental Subduction in Central Tibet and Mediterranean-Style Closure of the Paleo-Tethys Ocean. *Geology* **2008**, *36*, 351–354. [CrossRef]
66. Gehrels, G.E.; DeCelles, P.G.; Ojha, T.P.; Upreti, B.N. Geologic and U-Pb Geochronologic Evidence for Early Paleozoic Tectonism in the Dadeldhura Thrust Sheet, Far-West Nepal Himalaya. *J. Asian Earth Sci.* **2006**, *28*, 385–408. [CrossRef]
67. Gehrels, G.E.; DeCelles, P.G.; Ojha, T.P.; Upreti, B.N. Geologic and U-Th-Pb Geochronologic Evidence for Early Paleozoic Tectonism in the Kathmandu Thrust Sheet, Central Nepal Himalaya. *GSA Bull.* **2006**, *118*, 185–198. [CrossRef]
68. Veevers, J.J.; Saeed, A.; Belousova, E.A.; Griffin, W.L. U-Pb Ages and Source Composition by Hf-Isotope and Trace-Element Analysis of Detrital Zircons in Permian Sandstone and Modern Sand from Southwestern Australia and a Review of the Paleogeographical and Denudational History of the Yilgarn Craton. *Earth-Sci. Rev.* **2005**, *68*, 245–279. [CrossRef]
69. Morón, S.; Cawood, P.A.; Haines, P.W.; Gallagher, S.J.; Zahirovic, S.; Lewis, C.J.; Moresi, L. Long-Lived Transcontinental Sediment Transport Pathways of East Gondwana. *Geology* **2019**, *47*, 513–516. [CrossRef]
70. Clark, D.J.; Hensen, B.J.; Kinny, P.D. Geochronological Constraints for a Two-Stage History of the Albany–Fraser Orogen, Western Australia. *Precambrian Res.* **2000**, *102*, 155–183. [CrossRef]
71. Sircombe, K.N.; Freeman, M.J. Provenance of Detrital Zircons on the Western Australia Coastline—Implications for the Geologic History of the Perth Basin and Denudation of the Yilgarn Craton. *Geology* **1999**, *27*, 879–882. [CrossRef]
72. Dillinger, A.; George, A.D.; Parra-Avila, L.A. Early Permian Sediment Provenance and Paleogeographic Reconstructions in Southeastern Gondwana Using Detrital Zircon Geochronology (Northern Perth Basin, Western Australia). *Gondwana Res.* **2018**, *59*, 57–75. [CrossRef]
73. Haines, P.W.; Kirkland, C.L.; Wingate, M.T.D.; Allen, H.; Belousova, E.A.; Gréau, Y. Tracking Sediment Dispersal during Orogenesis: A Zircon Age and Hf Isotope Study from the Western Amadeus Basin, Australia. *Gondwana Res.* **2016**, *37*, 324–347. [CrossRef]

74. Kirkland, C.L.; Smithies, R.H.; Woodhouse, A.J.; Howard, H.M.; Wingate, M.T.D.; Belousova, E.A.; Cliff, J.B.; Murphy, R.C.; Spaggiari, C.V. Constraints and Deception in the Isotopic Record; the Crustal Evolution of the West Musgrave Province, Central Australia. *Gondwana Res.* **2013**, *23*, 759–781. [CrossRef]
75. Ameen, S.M.M.; Wilde, S.A. Multiple Sources for Archean Granitoids in the Yalgoo Area, Yilgarn Craton, Western Australia: Geochemical and Isotopic Evidence. *Precambrian Res.* **2018**, *314*, 76–110. [CrossRef]
76. Ivanic, T.J.; Van Kranendonk, M.J.; Kirkland, C.L.; Wyche, S.; Wingate, M.T.D.; Belousova, E.A. Zircon Lu–Hf Isotopes and Granite Geochemistry of the Murchison Domain of the Yilgarn Craton: Evidence for Reworking of Eoarchean Crust during Meso-Neoarchean Plume-Driven Magmatism. *Lithos* **2012**, *148*, 112–127. [CrossRef]